Int. J. Heat Mass Transfer. Vol. 16, pp. 1745–1761. Pergamon Press 1973. Printed in Great Britain

TRANSONIC LAMINAR BOUNDARY LAYERS WITH SURFACE CURVATURE*

LLOYD H. BACK
Jet Propulsion Laboratory Pasadena, California, U.S.A.

(*Received* 16 *February* 1971 *and in revised form* 13 *June* 1972)

Abstract—The effect of surface curvature (both longitudinal and transverse) and the associated pressure gradient across the flow is investigated analytically for a laminar boundary layer subjected to pressure gradients along the flow. Property variation which results from heat transfer and compressibility is taken into account. Numerical solutions of the boundary layer equations are obtained for locally similar sonic flow through the throat of a nozzle for a range of flow conditions and for various shaped nozzle surfaces with different amounts of wall cooling. A few solutions were also obtained for the analogous flow around the shoulder of a flat-faced body in a supersonic flow. The effect of various parameters that arise in the equations upon application of the Levy–Mangler transformation are investigated and discussed with respect to their influence on the velocity and total enthalpy profiles and the corresponding profile slopes at the surface to which the shear stress and heat transfer are related. An important finding is that at throat Reynolds numbers less than 10^5 the heat transfer parameter at a nozzle throat decreases as the throat radius of curvature decreases.

NOMENCLATURE

A, nozzle cross-sectional area;
C, density–viscosity product ratio, $\rho\mu/\rho_0\mu_0$;
c_f, friction coefficient;
D, nozzle diameter;
f', dimensionless velocity, u/U_0;
f_w'', friction parameter;
g, dimensionless total enthalpy, H_t/H_{to};
g_w, cooling parameter, H_w/H_{to};
G, dimensionless total enthalpy difference $(g - g_w)/(1 - g_w) = (H_t - H_w)/(H_{to} - H_w)$;
G_w', heat transfer parameter, $g_w'/(1 - g_w)$;
H, enthalpy;
H_t, total enthalpy, $H + u^2/2$;
k, thermal conductivity;
K, surface curvature parameter, equation (18);
$\dot{m}$, mass flow rate;
M, Mach number;
p, pressure;
Pr, Prandtl number;
q_w, heat flux to surface;
r, channel or body radius;
r_c, nozzle throat radius of curvature;
r_s, shoulder radius of curvature;
R, cylinder radius;
Re_D, throat Reynolds number, $(\rho_0 U_0 D/\mu_0)_{th}$;
S, flow speed parameter, equation (13);
St, Stanton number:
T, temperature;
u, v, components of velocity parallel and normal to surface;
U, V, free-stream velocity components;
x, distance along surface;
$\bar{x}$, length defined in equation (17);
y, distance normal to surface;
β, free-stream velocity . gradient parameter, equation (13);
γ, specific heat ratio;
δ, velocity boundary layer thickness;
δ_t, thermal boundary layer thickness;

* This work presents the results of one phase of research carried out in the Propulsion Research and Advanced Concepts Section of the Jet Propulsion Laboratory, California Institute of Technology, under Contract NAS7-100, sponsored by the National Aeronautics and Space Administration.

η, dimensionless coordinate normal to surface in transformed plane, equation (10);
θ, angle, Fig. 2;
$\varkappa$ surface curvature;
μ, viscosity;
ξ, coordinate along surface, equation (10);
ρ, density;
σ, convergent half angle of nozzle:
τ_w, surface shear stress.

Subscripts

aw, adiabatic surface condition;
i, inlet condition;
o, irrotational flow condition along surface;
t, stagnation condition;
th, throat condition;
w, surface condition.

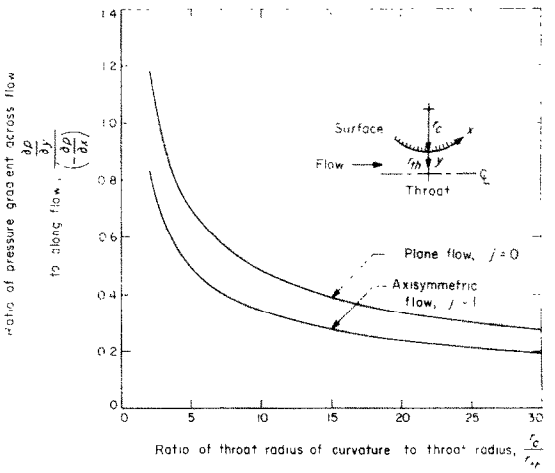

FIG. 1. Pressure gradients in the circular arc throat of a supersonic nozzle. The predictions are from the first approximation in the Hall solution [1], $\gamma = 1{\cdot}2$.

$$\frac{\partial p/\partial y}{(-\partial p/\partial x)} = \frac{\varkappa v}{\partial U/\partial x} = \left(\frac{\gamma+1}{1+j}\right)^{\frac{1}{2}}\left(1+\frac{1}{4}\frac{r_{th}}{r_c}\right)\left(\frac{r_{th}}{r_c}\right)^{\frac{1}{2}}$$

1. INTRODUCTION

IN THIS paper the effect of surface curvature (both longitudinal and transverse) on the shear stress and heat flux in laminar boundary layers is investigated analytically in the transonic region where the surface is usually curved and the heat transfer is often the highest. Specific examples of practical interest include nozzle throats and shoulder regions of blunt nosed bodies. Some idea of the relative magnitude of the pressure gradient across a curved flow compared to that along the flow is shown in Fig. 1 for isentropic flow through a nozzle with a circular-arc throat [1]. For rocket nozzles where the ratio of throat radius of curvature to throat radius r_c/r_{th} is of order unity, the pressure gradients are roughly the same in either direction.

After formulation of the problem, flow in the throat region of a nozzle is studied by obtaining similarity solutions for transonic flow of a perfect gas. Of specific interest is whether surface curvature increases or decreases the throat heat transfer and by how much. Such information is useful for example in rocket engine applications where nozzles with comparatively small radius of curvature throats and relatively steep convergent sections are presently being considered because they are shorter, weigh less and have a smaller surface area (and hence a lower total heat load). Attention is focussed on a laminar boundary layer because in previous nozzle heat transfer investigations [2, 3] it was found that steep convergence sections are advantageous for maintaining a laminar boundary layer or for laminarizing inlet turbulent boundary layers because of flow acceleration even though the Reynolds numbers may be fairly large, e.g. Re_D of 10^5–10^6. A small throat radius of curvature would also appear to be advantageous even if the boundary layer were turbulent since turbulence is apparently suppressed in flow over a convex surface [4]. A few calculations are also made at a shoulder of a flat-faced body where the boundary layer is usually laminar.

2. ANALYSIS

The laminar boundary layer equations for steady flow of a perfect gas along a curved

surface are as follows:

continuity:

$$\frac{\partial}{\partial x}[\rho u(r + iy\cos\theta)^j] + \frac{\partial}{\partial y}[(1 + \varkappa y) \times \rho v(r + iy\cos\theta)^j] = 0 \quad (1)$$

x-momentum:

$$\rho u\frac{\partial u}{\partial x} + (1 + \varkappa y)\rho v\frac{\partial u}{\partial y} + \rho\varkappa uv = -\frac{\partial p}{\partial x} + (1 + \varkappa y)\frac{\partial}{\partial y}\left(\mu\frac{\partial u}{\partial y}\right) - \varkappa u\frac{\partial \mu}{\partial y} + \mu\frac{\partial u}{\partial y}\left(\varkappa + \frac{ij\cos\theta}{r}\right) \quad (2)$$

y-momentum:

$$\rho\varkappa u^2 = (1 + \varkappa y)\frac{\partial p}{\partial y} \quad (3)$$

energy:

$$\rho u\frac{\partial H_t}{\partial x} + (1 + \varkappa y)\rho v\frac{\partial H_t}{\partial y} = (1 + \varkappa y)\frac{\partial}{\partial y} \times \left[\frac{\mu}{Pr}\frac{\partial H_t}{\partial y} + \mu\left(1 - \frac{1}{Pr}\right)\frac{\partial(u^2/2)}{\partial y}\right] - \varkappa\frac{y}{\partial y}(\mu u^2) + \left[\frac{\mu}{Pr}\frac{\partial H_t}{\partial y} + \mu \times \left(1 - \frac{1}{Pr}\right)\frac{\partial(u^2/2)}{\partial y}\right]\left(\varkappa + \frac{ij\cos\theta}{r}\right). \quad (4)$$

In these equations u and v are velocity components parallel and normal to the surface in the x and y direction, respectively, $\varkappa$ is the surface curvature and θ is the angle between the surface normal and body height (Fig. 2). The equations apply to axisymmetric flow with $j = 1$ and to flow over a plane surface with $j = 0$; for internal and external flows, $i = -1$ and 1, respectively. The equations are consistent with retaining terms involving $\varkappa$, $ij\cos\theta/r$ and include the effects of both longitudinal and transverse curvature. From the y-momentum equation, representing a balance between the pressure forces and centripetal acceleration, the role of surface curvature is clear (Fig. 2), e.g. for convex surfaces, $\varkappa$ is positive and the pressure increases outward from the surface.

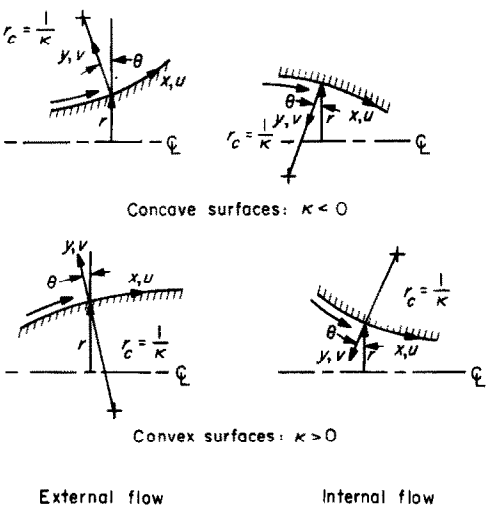

FIG. 2. Surface configurations and coordinates.

Equations (1)–(4) are coupled equations for ρ, u, v, H_t, p and μ when the surface shape is given, i.e. r, $\varkappa$ and θ are known. Specification of a viscosity relation $\mu(T)$, Prandtl number, pressure along the surface and boundary conditions complete the formulation.

For a surface impervious to flow and at a specified temperature so that the enthalpy at the surface is known, the surface conditions are

$$\text{at } y = 0;\ u = v = 0,\ H_t = H_w.$$

The external boundary condition for the total enthalpy for an adiabatic freestream flow is

$$\text{as } y \to \infty,\ H_t \to H_{to}\ \text{const.}$$

The velocity boundary condition is specified by applying the x-momentum equation in the freestream where viscous effects vanish

$$\rho U\frac{\partial U}{\partial x} + \rho V\frac{\partial}{\partial y}[(1 + \varkappa y)U] = -\frac{\partial p}{\partial x}. \quad (5)$$

The second and third terms in equation (2) were combined into one term as given in equation (5) since this term is one part of the irrotational condition for isentropic free-stream flow

$$\frac{\partial V}{\partial x} = \frac{\partial}{\partial y}[(1 + \varkappa y)U].$$

By taking the irrotational relation to be satisfied in the following sense

$$\frac{\partial}{\partial y}[(1 + \varkappa y)U] = 0 \tag{6}$$

the x-momentum equation (5) reduces to its usual form except that both the velocity U and pressure p depend on y as well as x

$$\rho U \frac{\partial U}{\partial x} = -\frac{\partial p}{\partial x}. \tag{7}$$

The external boundary condition on u from equation (6) then becomes

as $y \to \infty, u \to U$ where U is determined from

$$(1 + \varkappa y)\frac{\partial U}{\partial y} + \varkappa U = 0. \tag{8}$$

The pressure distribution is taken to be that associated with the external flow field and is obtained from the y- and x-momentum equations (3) and (7) since the velocity U from equation (6) becomes

$$U = \frac{U_0}{1 + \varkappa y} \tag{9}$$

where U_0 is the velocity along the surface for irrotational flow. This formulation though approximate is nevertheless consistent with the spirit of boundary layer theory since the boundary layer development is governed by the external flow field that is impressed on the fluid in the region near the surface, e.g. see Schultz-Grunow and Breuer [5] for an analysis for constant property, incompressible flow. The specific pressure distribution for transonic flow is considered in Section 3.

The equations are transformed from the x, y coordinates to the ξ, η coordinates by using a generalized Levy–Mangler transformation

$$\eta = \frac{r^{ij}U_0}{(2\xi)^{\frac{1}{2}}}\int_0^y \left(1 + ij\frac{y\cos\theta}{r}\right)\rho\,\mathrm{d}y;$$

$$\xi = \int_0^x \rho_0\mu_0 U_0 r^{2j}\,\mathrm{d}x. \tag{10}$$

Introduction of the stream function to satisfy the continuity equation and carrying out the transformation gives the following x-momentum and energy equations

$$\left[1 + K\left(1 + \frac{2ij\cos\theta}{\varkappa r}\right)\int_0^\eta \frac{\rho_0}{\rho}\,\mathrm{d}\eta\right]$$

$$\times (Cf'')' + ff'' + K\left[\frac{\rho_0}{\rho}ff' - \left(\frac{\mu}{\mu_0}\right)'f'\right]$$

$$+ K\left(1 + \frac{2ij\cos\theta}{\varkappa r}\right)\frac{\mu}{\mu_0}f''$$

$$+ \beta\left[\frac{\rho_0}{\rho}\left(-\frac{\partial p/\partial\xi}{\rho_0 U_0(\mathrm{d}U_0/\mathrm{d}\xi)}\right) - (f')^2\right]$$

$$= 2\xi\left(f'\frac{\partial f'}{\partial\xi} - f''\frac{\partial f}{\partial\xi} - K\frac{\rho_0}{\rho}f'\frac{\partial f}{\partial\xi}\right) \tag{11}$$

$$\left[1 + K\left(1 + \frac{2ij\cos\theta}{\varkappa r}\right)\int_0^\eta \frac{\rho_0}{\rho}\,\mathrm{d}\eta\right]\left(\frac{C}{Pr}g'\right)' + fg'$$

$$+ K\left(1 + \frac{2ij\cos\theta}{\varkappa r}\right)\left[\frac{\mu}{\mu_0}\frac{g}{Pr} + 2S\frac{\mu}{\mu_0}\right.$$

$$\left.\times\left(1 - \frac{1}{Pr}\right)f'f''\right] - 2KS\left[\frac{\mu}{\mu_0}(f')^2\right]'$$

$$+ S\left[1 + K\left(1 + \frac{2ij\cos\theta}{\varkappa r}\right)\int_0^\eta \frac{\rho_0}{\rho}\,\mathrm{d}\eta\right]$$

$$\times\left[2C\left(1-\frac{1}{Pr}\right)f'f''\right]' = 2\xi\left(f'\frac{\partial g}{\partial\xi}-g'\frac{\partial f}{\partial\xi}\right). \tag{12}$$

In these equations which are consistent with retaining terms involving $\varkappa$, $ij\cos\theta/r$ the velocity and total enthalpy have been normalized as $u/U_0 = f'$ and $H_t/H_{to} = g$, respectively. The primes denote partial differentiation with respect to η. The following abbreviations for quantities have been used:

$$C = \frac{\rho\mu}{\rho_0\mu_0};\ \beta = \frac{2\xi}{U_0}\frac{\mathrm{d}U_0}{\mathrm{d}\xi};\ K = \frac{\varkappa(2\xi)^{\frac{1}{2}}}{r^j\rho_0 U_0};\ S = \frac{U_0^2}{2H_{t0}} \tag{13}$$

The boundary conditions are as follows:

at the surface $\eta = 0$; $f = 0, f' = 0, g = g_w(\xi)$

in the free-stream $\eta \to \infty$;

$$\left(1 + K\int_0^\eta \frac{\rho_0}{\rho}\,\mathrm{d}\eta\right)f'' \to -Kf', g \to 1. \tag{14}$$

The heat flux to the surface and the surface shear stress can be written in the familiar form of the Stanton number and friction coefficient

$$St = \frac{q_w}{(H_{to} - H_w)(\rho_0 U_0)} = \frac{1}{(\rho_0 U_0\bar{x}/\mu_0)^{\frac{1}{2}}}\frac{C_w G'_w}{2^{\frac{1}{2}}Pr_w} \tag{15}$$

$$\frac{c_f}{2} = \frac{\tau_w}{\rho_0 U_0^2} = \frac{1}{(\rho_0 U_0\bar{x}/\mu_0)^{\frac{1}{2}}}\frac{C_w f''_w}{2^{\frac{1}{2}}} \tag{16}$$

In these expressions, $G'_w = g'_w/(1 - g_w)$, and the length $\bar{x}$ is defined by

$$\bar{x} = \frac{\xi}{\rho_0\mu_0 U_0 r^{2j}} = \frac{\int_0^x \rho_0\mu_0 U_0 r^{2j}\,\mathrm{d}x}{\rho_0\mu_0 U_0 r^{2j}}. \tag{17}$$

The parameter K can also be written in a form that indicates its basic dependence on $\varkappa\bar{x}$ and length Reynolds number

$$K = 2^{\frac{1}{2}}\frac{(\varkappa\bar{x})}{(\rho_0 U_0\bar{x}/\mu_0)^{\frac{1}{2}}}. \tag{18}$$

3. LOCAL SIMILARITY AND TRANSONIC FLOW

Surface curvature effects are investigated in accelerating flows over cooled surfaces with the similarity assumption i.e. $u/U_0 = f'(\eta)$ and $H_t/H_{to} = g(\eta)$, for which the terms on the right side of equations (11) and (12) are zero and which implies that the coefficients on the left side of equations (11) and (12) are invariable with ξ. Although such a situation is usually not found for flows over various shaped surfaces, similarity solutions are nevertheless useful since predictions with and without the similarity assumption have been found to differ by a small amount for accelerated flow over cooled surfaces where surface curvature was neglected, e.g. Marvin and Sinclair [6], when the boundary layer equations are transformed by the Levy–Mangler transformation as done herein. In the local similarity approach, a method suggested earlier by Lees [7] to predict heat transfer and later by Back and Witte [8] for accelerated flows with a large free-stream velocity gradient parameter β, the boundary layer profiles at a position along the surface are assumed to be the same as the similar profiles that would exist for the local free-stream condition.

Transonic flow is investigated by taking the mass flux in the external flow to be invariable, i.e. $\rho U = (\rho U)_0$ since the mass flux does not change with Mach number at the sonic condition, $M_0 = 1$. The pressure gradient across the flow from equation (3) can then be written as follows by using equation (9) for the external velocity U

$$\frac{\partial p}{\partial y} = \frac{(\rho U)_0\varkappa U_0}{(1 + \varkappa y)^2}.$$

Integration of this expression across the flow gives the following relation

$$p = -\frac{(\rho U)_0 U_0}{(1 + \varkappa y)} + \text{const.} \tag{19}$$

The pressure gradient along the flow is then obtained from this relation or from equation (7) as follows when the surface curvature is invariable

$$\frac{\partial p}{\partial \xi} = -\frac{(\rho U)_0 (dU_0/d\xi)}{(1 + \varkappa y)}$$

where

$$1 + \varkappa y = 1 + K \int_0^\eta \frac{\rho_0}{\rho} d\eta$$

in the transformed coordinate.

The calculations are carried out for a perfect gas with viscosity proportional to temperature and a Prandtl number of unity. The viscosity ratio is then directly related to the temperature ratio, and thus g and f'.

$$\frac{\mu}{\mu_0} = \frac{T}{T_0} = \left(1 + \frac{\gamma - 1}{2} M_0^2\right) g - \frac{\gamma - 1}{2} \times M_0^2 (f')^2.$$

The density ratio is taken to be inversely proportional to the temperature ratio, $\rho_0/\rho = T/T_0$ and consequently $C = 1$, since for the flows considered the magnitude of the pressure change across the boundary layer is not large even though the pressure gradient is significant. The actual pressure variation would be less than that given by the following relation obtainable from equation (19)

$$\frac{p}{p_0} = 1 + \gamma M_0^2 \frac{\varkappa y}{(1 + \varkappa y)}.$$

The form of the boundary layer equations (11) and (12) consistent with these considerations is as follows:

$$\left[1 + K\left(1 + \frac{2ij\cos\theta}{\varkappa r}\right) \int_0^\eta \frac{T}{T_0} d\eta\right] f''' + ff'' + K\left[\frac{T}{T_0} ff' - \left(\frac{T}{T_0}\right)' f'\right] + K\left(1 + \frac{2ij\cos\theta}{\varkappa r}\right) \frac{T}{T_0} f'' + \beta\left[\frac{T}{T_0} \frac{1}{\left(1 + K \int_0^\eta \frac{T}{T_0} d\eta\right)} - (f')^2\right] = 0 \tag{20}$$

$$\left[1 + K\left(1 + \frac{2ij\cos\theta}{\varkappa r}\right) \int_0^\eta \frac{T}{T_0} d\eta\right] G'' + fG' + K\left(1 + \frac{2ij\cos\theta}{\varkappa r}\right) \frac{T}{T_0} G' - \frac{2KS}{(1 - g_w)} \left[\frac{T}{T_0} (f')^2\right]' = 0. \tag{21}$$

The enthalpy difference ratio $G = (g - g_w)/(1 - g_w)$ was introduced so that values of G range from 0 at the surface, taken to be isothermal, to 1 in the free-stream.

4. NOZZLE THROAT

Some idea of the dependence of the parameters K and β on flow conditions and configuration in the throat region of an axisymmetric supersonic nozzle is established by taking the external flow to be approximately one-dimensional for which ξ is given by

$$\xi = \int_0^x \rho_0 \mu_0 U_0 r^2 \, dx = (\rho_0 U_0 r^2) \int_0^x \mu_0 \, dx = \frac{\dot{m}}{\pi} \mu_0 \bar{x}$$

where $\dot{m}$ is the mass flow rate and $\bar{x}$ is the length along the nozzle weighed by the viscosity in accordance with the transformation

$$\bar{x} = \frac{1}{\mu_0} \int_0^x \mu_0 \, dx.$$

For a nozzle with a circular arc throat, $r_c = 1/\varkappa$, the surface curvature parameter K (equation (18)) can be rewritten at the throat as follows

$$K_{th} = \frac{2}{(r_c/r_{th})} \frac{(\bar{x}/r)_{th}^{\frac{1}{2}}}{Re_D^{\frac{1}{2}}} \text{ where } Re_D = \left(\frac{\rho_0 U_0 D}{\mu_0}\right)_{th}. \tag{22}$$

The parameter K_{th} increases as the throat Reynolds number decreases: it also increases for a nozzle with a smaller throat radius of curvature, i.e. smaller r_c/r_{th}, and as the relative distance to the throat $(\bar{x}/r)_{th}$ increases. For nozzle shapes and flows of practical interest, values of K_{th} are not large as will be seen.

The free-stream velocity gradient parameter β for one-dimensional flow is

$$\beta = \frac{2}{U_0}\frac{dU_0}{dx}\left(\frac{\xi}{d\xi/dx}\right) = -\frac{(4/r)(dr/dx)}{(1-M_0^2)}\bar{x}.$$

At the throat where the flow is sonic, β is given by

$$\beta_{th} = \frac{2}{[(\gamma+1)/2]^{\frac{1}{2}}} \frac{(\bar{x}/r)_{th}}{(r_c/r_{th})^{\frac{1}{2}}}. \tag{23}$$

The parameter β_{th} is generally larger than unity and increases as r_c/r_{th} decreases or as $(\bar{x}/r)_{th}$ increases.

The following relations complete the specification of flow through a nozzle throat

$$\left(1 + \frac{2ij\cos\theta}{\varkappa r}\right) = 1 - \frac{2r_c}{r_{th}}$$

$$S = \frac{\gamma-1}{2}\frac{M_0^2}{1+[(\gamma+1)/2]^{\frac{1}{2}}M_0^2} = \frac{\gamma-1}{\gamma+1}$$

$$\frac{T}{T_0} = \frac{\gamma+1}{2}[G(1-g_w)+g_w] - \frac{\gamma-1}{2}(f')^2.$$

Insertion of the preceding relations into equations (20) and (21) indicate a dependence of the velocity and total enthalpy profiles upon the following parameters: r_c/r_{th}, g_w, γ and K, β or $(\bar{x}/r)_{th}$, Re_D. A description of the method used to solve these equations appears in the appendix.

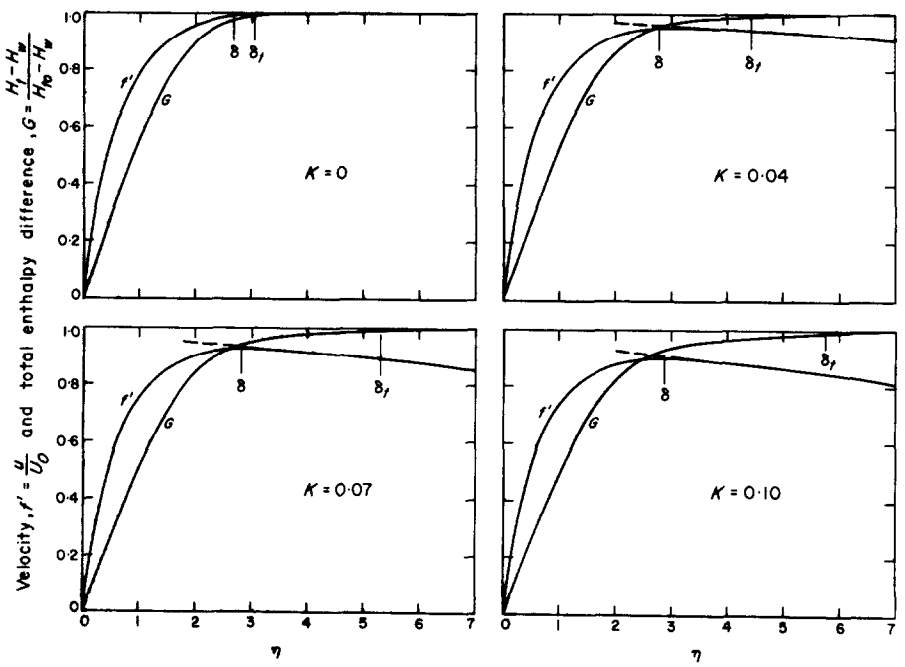

FIG. 3. Effect of the surface curvature parameter on the velocity and total enthalpy profiles at a nozzle throat in the transformed plane: $M_0 = 1$, $\beta = 9{\cdot}1$, $r_c/r_{th} = 0{\cdot}25$, $g_w = 0{\cdot}2$, $\gamma = 1{\cdot}2$.

The effect of the surface curvature parameter K on the velocity and total enthalpy profiles at the throat of a nozzle of given shape, i.e. fixed r_c/r_{th} and β, is shown in Fig. 3 in the transformed plane for a high temperature gas flow ($\gamma = 1{\cdot}2$) with wall cooling, $g_w = 0{\cdot}2$. The profiles correspond to different values of K whose variation is then determined by operating conditions, i.e. Reynolds number (equation (22)). The profiles for a limiting value of $K \to 0$ are associated with an infinite Reynolds number flow and are identical to those profiles that have been obtained by not taking curvature effects into account [9]. This indeed should be the case since in this limit equations (20) and (21) take on the usual form of the transformed boundary layer equations, e.g. [9], although the external boundary condition, equation (14) is $f'' \to 0$, rather than $f' \to 1$. This coincidence in the profiles as well as their slopes at the surface for $K \to 0$ establishes some confidence in the present method of numerically solving the equations. As K is increased, i.e. decreasing Reynolds number, the velocity profiles become less steep near the surface, although this is difficult to discern in Fig. 3. The total enthalpy profiles also become less steep near the surface as K increases, but like the velocity profiles, the relative decrease in the profile slopes at the surface is better seen in a subsequent representation. In the outer part of the boundary layer the velocity profiles are depressed because of the curvature of the convex throat which reduces the external velocity away from the surface. This smaller velocity difference across the boundary layer is believed to be primarily responsible for the reduction in the slope of the velocity profile near the surface.

The profiles are shown for values of K to 0·1 in Fig. 3. Even though this value is relatively small there may be some question about retaining terms involving only $\varkappa$, and not $\varkappa^2$, in the original equations. It turns out, however, that this limitation is generally within the realm of interest for nozzle throat flows as will be seen subsequently. For example, the edge of the velocity boundary layer δ is about at $\eta \simeq 2{\cdot}9$ for the profile at $K = 0{\cdot}1$. The ratio of δ to throat radius of curvature r_c, $\delta/r_c = \kappa\delta = K \int_0^{\eta \simeq 3} (T/T_0)\, d\eta$ the κ is 0·20 and $(\kappa\delta)^2$ would be 0·04.

It appears in Fig. 3 that the thermal layer thickness δ_t exceeds the velocity layer thickness δ, more so as K increases, although there is difficulty in assigning specific values to either thickness, or for that matter the displacement thickness. The apparent thickening of the thermal layer as K increases probably is responsible for the reduced slope of the total enthalpy profile at the surface that is observed. The displacement effect is expected to be small at a nozzle throat because the combined effects of acceleration and cooling reduce the displacement thickness [9]. In fact, with a significant amount of wall cooling the mass flux through the boundary layer can exceed the external flow value and for this situation the displacement thickness is negative, as it is for the conditions shown in Fig. 3 for $K \to 0$. Even for an adiabatic surface the displacement effect is small in the Reynolds number range of interest as indicated by the measurements in [10].

The important quantities from which the surface shear stress and heat flux can be calculated—the profile slopes at the surface, f_w'' and G_w'—are shown in Fig. 4. These quantities that correspond to the profiles previously discussed will be referred to as the friction and heat transfer parameters. Both of these parameters decrease with K. Over the range of K indicated, the decrease in the friction parameter is not very much, although the decrease in the heat transfer parameter is somewhat larger. The trend whereby f_w'' and G_w' decrease with K, essentially in a linear way, is consistent with that obtained from previous calculations for low speed, constant property flows over convex surfaces with heat transfer (Van Dyke [11] and Schultz-Grunow and Breuer [5]) and the recent survey of higher order boundary layer theory by Van Dyke [12]. Previous calculations for high speed flows over convex bodies including

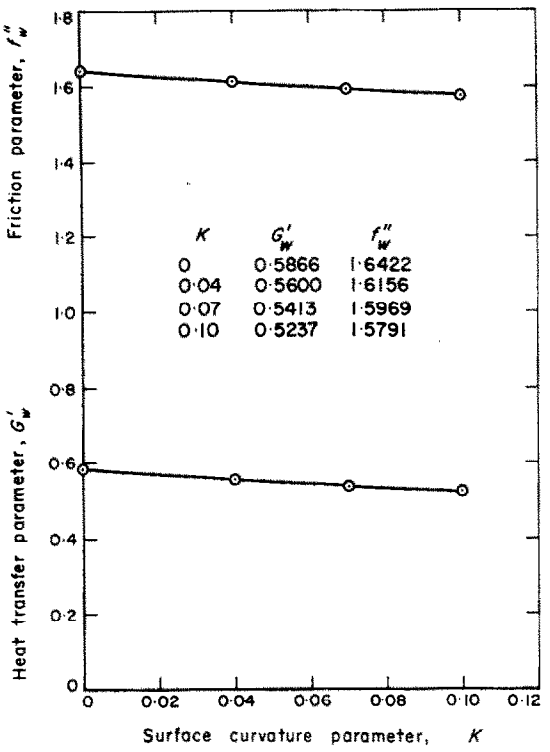

FIG. 4. Effect of the surface curvature parameter on the heat transfer and friction parameters at a nozzle throat: $M_0 = 1$, $\beta = 9{\cdot}1$, $r_c/r_{th} = 0{\cdot}25$, $g_w = 0{\cdot}2$, $\gamma = 1{\cdot}2$.

heat transfer, e.g. see the earlier survey by Van Dyke [13] (Refs. [14–19]) and more recent calculations [20–22], and the recent survey by Van Dyke [12], reveal a more complicated behavior that is dependent upon the many considerations in these analyses i.e. interactions with the external flow and non-continuum surface phenomena, in addition to longitudinal and transverse surface curvature, amount of wall cooling, and location along the body.

To appraise the influence of throat configuration it is convenient to select a particular contraction area ratio for a nozzle A_i/A_{th}, and contraction section length which for a conical nozzle with a relatively small length of throat section is given approximately by

$$\left(\frac{x}{r}\right)_{th} \cong \frac{(r_i/r_{th}) - 1}{\sin\sigma}$$

where σ is the conical half-angle. The effect of varying the throat radius of curvature can then be investigated, i.e. r_c/r_{th}, at various Reynolds numbers or operating conditions. Table 1 gives the corresponding values of the parameters K and β calculated from equations (22) and (23) for the specific values of A_i/A_{th} and γ indicated ($\bar{x}$ was taken approximately equal to x since these lengths would only differ by a small amount). The friction and heat transfer parameters so obtained from the solution of the boundary layer equations are shown in Fig. 5 for nozzles with a conical half angle of 75° and wall cooling, $g_w = 0{\cdot}2$.

The frction parameter is seen to increase significantly as the throat radius of curvature becomes smaller. This occurs primarily because

Table 1. *Nozzle throat parameters:* $M_0 = 1$, $A_i/A_{th} = 10$, $\gamma = 1{\cdot}2$

	$\sigma = 75°$				$\sigma = 45°$	
$\frac{r_c}{r_{th}}$	β	$Re_D = 10^3$ K	10^5 K	$\to\infty$ K	β	$Re_D = 10^5$ K
0·125	12·1	—	0·076	0	16·4	0·089
0·25	8·54	0·38*	0·038	0		
0·50	6·04	0·19	0·019	0		
0·75	4·93	0·13	0·013	0	6·73	0·015
1·0	4·27	0·095	0·0095	0		
1·5	3·49	0·063	0·0063	0		
2·0	3·02	0·048	0·0048	0	4·12	0·0055

* Terms involving K^2 not considered, may become important.

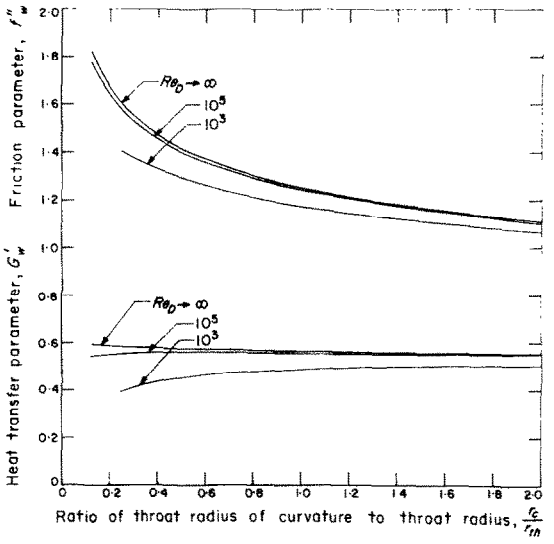

FIG. 5. Effect of nozzle throat curvature on the heat transfer and friction parameters at various Reynolds numbers. $M_0 = 1, A_i/A_{th} = 10, \sigma = 75°, g_w = 0{\cdot}2, \gamma = 1{\cdot}2$.

the velocity profile is strongly dependent upon the free-stream velocity gradient parameter β in accelerated flows (e.g. [9] wherein the free-stream velocity gradient parameter $\bar{\beta}$ is related to β by $\beta = [2/(\gamma + 1)]\bar{\beta}$ for sonic flow). As β increases, as it does with smaller throat radius of curvature, so does the slope of the velocity profile at the surface f''_w. The effect of the surface curvature parameter K however leads to a decrease in f''_w for a smaller throat radius of curvature, but this decrease is relatively small compared to the increase with β. Although the friction parameter does increase for a nozzle with a smaller throat radius of curvature, the result is not particularly significant, except perhaps for an ablative throat, since the contribution of the viscous shear forces is usually small compared to pressure forces acting on the nozzle surface unless the Reynolds number is relatively low, and consequently the reduction in nozzle thrust would be small.

Of more importance is the heat transfer in the throat vicinity. As indicated in Fig. 5, the heat transfer parameter, unlike the friction parameter, can decrease with a smaller throat radius of curvature. This behavior occurs because the slope of the total enthalpy profile at the surface G'_w increases much less with β than the slope of the velocity profile at the surface f''_w [9] and consequently at lower Reynolds numbers can be offset by the decrease of G'_w with K as the throat radius of curvature becomes smaller. This finding is of significance since it would appear that the design of a nozzle with a relatively small throat radius of curvature would lead to a reduction in heat transfer at lower Reynolds numbers relative to that value predicted by not taking into account surface curvature in the solution of the boundary layer equations, i.e. $K \to 0$, which corresponds to the infinite Reynolds number limit. Of course, the throat heat flux depends on other quantities (equation (15)) in addition to G'_w, e.g. for a given stagnation temperature, it also decreases with decreasing Reynolds number or mass flux, a situation also found for the surface shear stress (equation (16)).

Some support for the predicted reduction in throat heat transfer because of surface curvature is afforded by the heat transfer measurements in [23] which were conducted with argon ($\gamma = \frac{5}{3}$) at very high temperatures up to 14 000°R flowing through a highly cooled nozzle ($g_w = 0{\cdot}04$). Numerical calculations involving the viscous, heat conducting laminar flow equations without curvature terms were carried out in conjunction with the experiments. Good agreement was found between the measured and predicted heat flux along the conical convergent section of the nozzle, $\sigma = 10°$, $A_i/A_{th} = 10{\cdot}6$, $K = 0$, but through the circular arc throat region ($r_c/r_{th} = 4$) the measured heat flux decreased more rapidly than the predicted value. Application of the calculations herein to the throat flow, $Re_D \cong 2000$, $\beta = 11{\cdot}3$ and $K = 0{\cdot}04$, indicated a predicted reduction in G'_w of 15 per cent below the case of $K \to 0$. This lower predicted value of G'_w and thus the heat flux, is consistent with the trend of the data although the aforementioned viscous flow calculations were in fair agreement in magnitude with the measurements on an average basis through the circular throat region.

It should be mentioned that the magnitude of the reduction in G'_w predicted for this nozzle with a larger r_c/r_{th} than considered in the previous calculations is associated with the lower throat Reynolds number of 2000 of the very high temperature gas flow (the term $K\ (1 - 2r_c/r_{th})$ in equations (20) and (21) is apparently significant and depends only on Re_D for a nozzle with a given contraction area ratio and conical half angle as r_c/r_{th} becomes larger).

[9]. Since β also increases with a longer contraction section length, i.e. smaller σ, the heat transfer and friction parameters increase as well, but again the effect is larger for the friction than the heat transfer parameter.

The calculations could be carried out for nozzles with other shapes of interest and be refined perhaps for fairly steep convergence section nozzles where the one-dimensional flow assumption used herein to explore surface

Table 2. Heat transfer and friction parameters, G'_w and f''_w at a nozzle throat: $M_0 = 1$, $A_i/A_{th} = 10$, $\gamma = 1{\cdot}2$

	$\sigma = 75°$								$\sigma = 45°$	
$\frac{r_c}{r_{th}}$	$Re_D = 10^3$		$Re_D = 10^5$				$Re_D \to \infty$		$Re_D = 10^5$	
	$g_w = 0{\cdot}2$		$g_w = 0{\cdot}2$		$g_w = 0{\cdot}6$		$g_w = 0{\cdot}2$		$g_w = 0{\cdot}2$	
	G'_w	f''_w	G'_w	f''_w	G'_w	f''_w	G'_w	f''_w	G'_w	f''_w
0·125	—	—	0·5465	1·7791	0·5477	3·0489	0·5935	1·8263	0·5456	1·9958
0·25	0·3928	1·4086	0·5598	1·5801			0·5851	1·6053		
0·50	0·4546	1·2950	0·5622	1·4028			0·5761	1·4166		
0·75	0·4761	1·2249	0·5602	1·3087	0·5969	2·0449	0·5705	1·3189	0·5670	1·4598
1·0	0·4901	1·1786	0·5584	1·2465			0·5665	1·2545		
1·5	0·5014	1·1122	0·5546	1·1650			0·5607	1·1711		
2·0	0·5050	1·0644	0·5513	1·1103	0·5880	1·6479	0·5565	1·1156	0·5594	1·2327

The solutions shown so far were obtained for a specific amount of wall cooling $g_w = 0{\cdot}2$ and for a particular contraction section shape as specified by the conical half-angle σ. In Table 2 the heat transfer and friction parameters are shown to indicate the effect of wall cooling and the contraction section length. These results obtained for a throat Reynolds number of 10^5 display the same general trends with throat radius of curvature as previously observed in Fig. 5. For less wall cooling, i.e. larger g_w, both the heat transfer and friction parameters increase, although the effect is greater on the friction parameter than the heat transfer parameter. This behavior is primarily associated with the effect of acceleration, i.e. β, which causes a progressively wider variation of the friction and heat transfer parameters with the amount of wall cooling as β increases. At a particular value of β, f''_w and G'_w increase with less wall cooling

curvature effects becomes less realistic. It should be noted that the flow along the surface is sonic upstream of the physical throat, e.g. see the measurements in [24].

5. BLUNT BODY SHOULDER SOLUTIONS

A few calculations were made in the transonic region for a flat-faced axisymmetric body with a circular arc shoulder in a supersonic flow. The surface pressure measurements of Marvin and Sinclair [6] indicate that as the ratio of the shoulder radius of curvature to the cylinder radius downstream r_s/R becomes smaller (0·05 being the smallest ratio investigated) the sonic point moves toward the beginning of the shoulder section and for this situation the angle θ between the surface normal and body radius approaches 90° (Fig. 2). Therefore, the term $1 + 2\cos\theta/\varkappa r$ becomes 1 as also would be the

case since $1/\varkappa r = r_s/r$ is small. For the smallest value of r_s/R of 0·05 which should correspond to the largest effect of including curvature terms, the free-stream velocity gradient parameter β is about 10 at the sonic condition (Fig. 3 of [6]). The friction and heat transfer parameters that were calculated by numerically solving equations (20) and (21) for a cooled wall condition $g_w = 0{\cdot}25$, corresponding to Marvin and Sinclair's experiments with air with γ taken as 1·4, are shown in Fig. 6 for various values of the

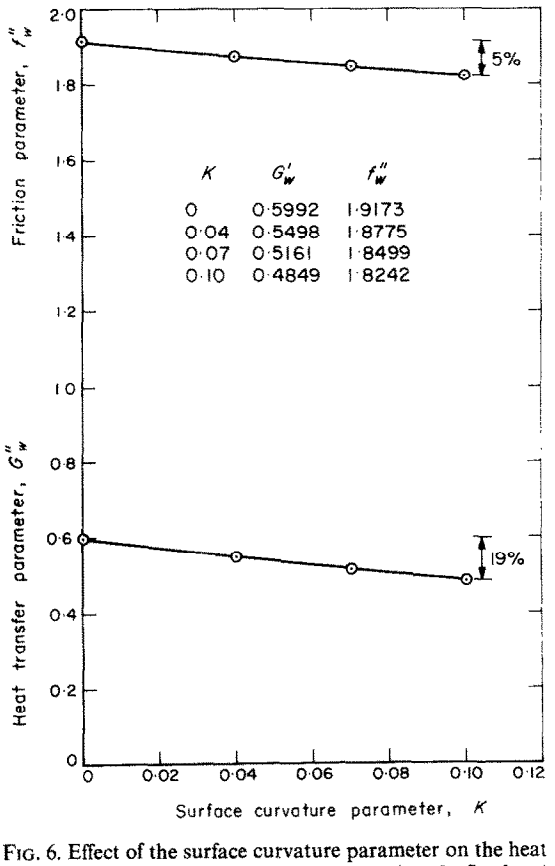

FIG. 6. Effect of the surface curvature parameter on the heat transfer and friction parameters at a shoulder of a flat faced body with a relatively small shoulder radius of curvature: $M_0 = 1$, $\beta = 10$, $g_w = 0{\cdot}25$, $\gamma = 1{\cdot}4$.

surface curvature parameter K. The trend indicated in Fig. 6 is similar to that found at the throat of a nozzle although the reduction in G'_w for the same value of K is larger. Marvin and Sinclair's experiments were conducted at only one stagnation condition, and the corresponding value of K from equation (18) at the sonic condition for the smallest ratio of $r_s/R = 0{\cdot}05$ is 0·042. From Fig. 6, the reduction in the heat transfer parameter G'_w below the value associated with neglecting surface curvature effects, i.e. $K \to 0$, is 9 per cent at this value of K. This somewhat smaller value of G'_w would be in better agreement with the heat transfer measurements that were made (Fig. 4 of [6] for $r_s/R = 0{\cdot}05$) since the locally similar solutions with curvature terms not taken into account overestimated the measured peak heat flux in the transonic region by about 10 per cent. This better agreement, however, might be somewhat fortuitous because of the accuracy of the heat flux measurements in the small shoulder region and the fact that the locally similar solutions without curvature terms were already about 10 per cent below a more exact calculation of the peak heat flux that involved retaining the non-similar terms in the boundary layer equations. Nevertheless, the predicted trend of lower heat transfer appears to be consistent with the measurements.

6. OTHER CONSIDERATIONS

To apply the similarity solutions to real gas flows with viscosity not proportional to temperature and Prandtl number not equal to unity, about the only heat transfer correction that would appear worthwhile making for transonic flow is to set Pr_w and C_w equal to unity in the Stanton number relation equation (15), consistent with the present values for G'_w, and then replace St by $StPr^{\frac{2}{3}}$, i.e.

$$StPr^{\frac{2}{3}} = \frac{1}{(\rho_0 U_0 \bar{x}/\mu_0)^{\frac{1}{2}}} \frac{G'_w}{2^{\frac{1}{2}}}. \qquad (24)$$

Otherwise the predicted heat flux would be too low when the Prandtl number is less than unity which is the case for most gases. A corresponding correction for a more appropriate driving potential between adiabatic wall and wall en-

thalpies would be small for transonic flow. For example at the sonic condition, the ratio of adiabatic wall enthalpy to stagnation enthalpy is 0·985 if the recovery factor is 0·83 and specific heat ratio is 1·2. For transonic flow, the friction coefficient might also be obtained from equation (16) as follows, consistent with the present values of f_w'' for C equal to unity

$$\frac{c_f}{2} = \frac{1}{(\rho_0 U_0 \bar{x}/\mu_0)^{\frac{1}{2}}} \frac{f_w''}{2\frac{1}{2}}. \tag{25}$$

These suggestions are based on differences in the heat transfer and friction relations that have been predicted (not including curvature terms) for real gases for which the viscosity dependence on temperature is usually less than linear, e.g. for the empirical relation $\mu \alpha T^{\omega}$, $\omega < 1$. The general trends whereby values of ω less than unity lead to increases in the heat transfer and friction relations with wall cooling while increases in flow speed (compressibility) reduce the heat transfer and friction relations that have been found for flows with relatively small values of the free-stream velocity gradient parameter β, e.g. see Table 3 of [9], apparently also are predicted in flows with larger values of $\bar{\beta}$ such as considered herein as indicated by the recent similarity calculations in [25]. However, for transonic flow these opposing trends tend to cancel one another and apparently would not change the heat transfer and friction relations much.

7. SUMMARY AND CONCLUSIONS

The effect of surface curvature on the flow and heat transfer in laminar boundary layers was investigated by application of the Levy–Mangler transformation to an appropriate form of the boundary layer equations and by studying the effect of various parameters that influence the velocity and total enthalpy profiles and thus their slopes at the surface f_w'' and G_w' to which the shear stress and heat transfer are related. Numerical solutions of the integro-differential equations were obtained for a locally similar sonic flow in the throat region of various shaped nozzles with wall cooling over a range of flow conditions. The velocity profiles become depressed in the outer part of the boundary layer because of the curvature of the convex throat which reduces the external velocity away from the surface. The friction and heat transfer parameters f_w'' and G_w' decrease essentially in a linear way with the surface curvature parameter K, and this change is believed to be primarily caused by a smaller velocity difference across the boundary layer and an apparent thickening of the thermal layer, respectively.

Application of the analysis to nozzles with different throat radii of curvature indicated that a small throat radius of curvature would lead to a reduction in the heat transfer parameter at lower Reynolds numbers. Some support for the predicted reduction in throat heat transfer because of surface curvature is inferred from the measurements in [23]. Even though the wall shear stress would significantly increase in a nozzle with a small throat radius of curvature, the reduction in nozzle thrust because of viscous shear forces would be relatively small and consequently not be of much importance except perhaps for an ablative throat. These trends arise because the heat transfer parameter G_w' is rather weakly dependent on the free-stream velocity gradient parameter β for acclerated flows with the increase G_w' with β offset by the decrease of G_w' with K. The friction parameter f_w'' however is strongly dependent on β, with the increase with β overwhelming the decrease with K. Both of the parameters f_w'' and G_w' increase with less wall cooling and a longer contraction section length primarily because of the simultaneous effects of cooling and acceleration.

There however may be an increase in heat transfer downstream of the throat as the throat radius of curvature is made smaller since the boundary layer may be subjected to an adverse pressure gradient as was noted in [26] just downstream of the tangency of the circular arc throat $r_c/r_{th} = 0{\cdot}625$ and conical divergent section (15 deg half angle). This adverse pressure

gradient which is believed to be associated with a compressive turning of the flow that acquires a strong angular motion in the small-radius-of-curvature throat region, can separate the boundary layer and lead to an increase in heat transfer downstream of the throat [3, 26]. It is difficult to determine a precise value for r_c/r_{th} to avoid this adverse pressure gradient which would also depend to some extent on the nozzle shape downstream. Available experimental information for nozzles with a conical half-angle of divergence of 15° [26–28] indicate that r_c/r_{th} should probably not be made smaller than a value of about 0·75.

Similar trends for the friction and heat transfer parameters, i.e. their decrease with K, were also predicted for the analogous flow around shoulders of blunt-nosed bodies in supersonic flow. Reasonable agreement was found with the heat transfer measurements of Marvin and Sinclair [6] for a flat-faced axisymmetric body with a relatively small shoulder radius of curvature.

ACKNOWLEDGEMENT

The author expresses his gratitude to P. Breckheimer (of JPL) for programming the numerical technique used to solve the equations and for carrying out the numerical calculations on a UNIVAC 1108 computer.

REFERENCES

1. I. M. Hall, Transonic flow in two-dimensional and axially-symmetric nozzles, *Q. J. Mech. Appl. Math.* **15**, Part 4, 487–508 (1962).
2. L. H. Back, P. F. Massier and R. F. Cuffel, Some observations on reduction of turbulent boundary layer heat transfer in nozzles, *AIAA Jl* **4**, 2226–2229 (1966).
3. L. H. Back, P. F. Massier and R. F. Cuffel, Effect of inlet boundary layer thickness and structure on heat transfer in a supersonic nozzle, *J. Spacecraft Rockets* **5** (1), 121–123 (1968).
4. H. Thomann, Effect of streamwise wall curvature on heat transfer in a turbulent boundary layer, *J. Fluid Mech.* **33** (2), 283–292 (1968).
5. F. Schultz-Grunow and W. Breuer, Laminar boundary layers on cambered walls, *Basic Developments in Developments in Fluid Dynamics*, edited by M. Holt, Vol. 1. Academic Press (1965).
6. J. G. Marvin and A. R. Sinclair, Convective heating in regions of large favorable pressure gradient, *AIAAJl* **5**, 1940–1948 (1967).
7. L. Lees, Laminar heat transfer over blunt-nosed bodies at hypersonic flight speeds, *Jet Propul.* **26**, 259–269 (1956).
8. L. H. Back and A. B. Witte, Prediction of heat transfer from laminar boundary layers, with emphasis on large free-steam velocity gradients and highly cooled walls, *J. Heat Transfer* **88C**, 249–256 (1966).
9. L. H. Back, Acceleration and cooling effects in laminar boundary layers—subsonic, transonic and supersonic speeds, *AIAA Jl* **8** (4), 794–802 (1970).
10. P. F. Massier, L. H. Back, M. B. Noel and F. Saheli, Viscous effects on the flow coefficient for a supersonic nozzle, *AIAA Jl* **8** (3), 605–607 (1970).
11. M. Van Dyke, Higher approximations in boundary layer theory, Part 2, Application to leading edges, *J. Fluid Mech.* **14**, 481–495 (1962).
12. M. Van Dyke, Higher order boundary layer theory, *Annual Review of Fluid Mechanics*, edited by W. R. Sears and M. Van Dyke, Vol. 1, pp. 265–292. Annual Reviews, Palo Alto, California (1969).
13. M. Van Dyke, A Survey of higher-order boundary layer theory, Report SUDAAR-326, Dept. of Aeronautics and Astronautics, Stanford Univ. (Sept. 1967). [Also AFOSR Scientific Report AFOSR-67-2291 and presented at AGARD Seminar on Numerical Methods for Viscous Flows, National Physical Laboratory, Teddington, England (18–21 Sept. 1967).]
14. M. Van Dyke, Second-order compressible boundary layer theory with application to blunt bodies in hypersonic flow, *Hypersonic Flow Research*, edited by F. R. Riddell, pp. 37–76. Academic Press, New York (1962).
15. S. H. Maslen, Second-order effects in laminar boundary layers, *AIAA Jl* **1** (1), 33–40 (1963).
16. R. T. Davis and I. Flugge-Lotz, The laminar compressible boundary layer in the stagnation-point region of an axisymmetric blunt body including the second-order effect of vorticity interaction, *Int. J. Heat Mass Transfer* 7, 341–370 (1964).
17. R. T. Davis and I. Flugge-Lotz, Second-order boundary layer effects in hypersonic flow past axisymmetric blunt bodies, *J. Fluid Mech.* **20** (4), 593–623 (1964).
18. T. K. Fannelop and I. Flugge-Lotz, Two-dimensional hypersonic stagnation flow at low Reynolds numbers, *Z. Flugwiss.* **13**, 282–296 (1965).
19. T. K. Fannelop and I. Flugge-Lotz, Viscous hypersonic flow over simple blunt bodies; comparison of a second-order theory with experimental results, *J. Mécanique* **5**, 69–100 (1966).
20. J. C. Adams Jr., Higher order boundary layer effects on analytic bodies of revolution, Arnold Engineering Development Center, AEDC-TR-68-57, Tennessee (April 1968). Also presented at AGARD Seminar on Numerical methods for viscous flows, National Physical Laboratory, Teddington, England (18–21 Sept. 1967).
21. C. H. Lewis, First- and second-order boundary-layer effects at hypersonic conditions, (Paper presented at AGARD Seminar on Numerical methods for viscous flows, National Physical Laboratory, Teddington, England (18–21 Sept. 1967).
22. C. H. Lewis, Computation of higher-order boundary layer effects with a first-order treatment and compari-

son with experimental data, *AIAA Paper* No. 70–185 (Jan. 1970).
23. L. H. BACK and P. F. MASSIER, Viscous, non-adiabatic laminar flow through a supersonic nozzle—experimental results and numerical calculations. *J. Heat Transfer* **94C**, 437–445 (1972).
24. R. F. CUFFEL, L. H. BACK and P. F. MASSIER, Transonic flow field in a supersonic nozzle with small throat radius of curvature, *AIAA Jl* 7 (7), 1364–1366 (1969).
25. A. WORTMAN and A. F. MILLS, Highly accelerated compressible laminar boundary layer flows with mass transfer, *J. Heat Transfer* **93** (3), 281–289 (1971).
26. L. H. BACK, P. F. MASSIER and R. F. CUFFEL, Flow phenomena and convective heat transfer in a conical supersonic nozzle, *J. Spacecraft Rockets* **4** (8), 1040–1047 (1967).
27. L. H. BACK, P. F. MASSIER and H. L. GIER, Comparison of measured and predicted flows through conical supersonic nozzles, with emphasis on the transonic region, *AIAA Jl* 3 (9), 1606–1614 (1965).
28. S. V. SHELTON, private communication.
29. J. P. KEENER, The numerical solution of two-point boundary value problems with linear boundary constraints, *Supporting Research and Advanced Development*, Space Programs Summary 37–60, Vol. III, pp. 4–9. Jet Propulsion Laboratory, Pasadena, California (Dec. 1969).
30. F. T. KROGH, VODQ/SVDQ/DVDQ—variable order integrators for the numerical solution of ordinary differential equations, Section 314 Subroutine Write-Up, Jet Propulsion Laboratory, Pasadena, California (May 1969).
31. R. J. HANSON, NWTR/NWTR2, Section 314 Subroutine Write-Up, Jet Propulsion Laboratory, Pasadena, California (Aug. 1969).
32. H. B. KELLER, *Numerical Methods for Two-Point Boundary Value Problems*, pp. 61–68. Blaisdell, Waltham, Massachusetts (1968).
33. S. D. CONTE, The numerical solution of linear boundary value problems, *SIAM Rev.* **8**, 309–321 (1966).
34. M. R. OSBORNE, On shooting methods for boundary value problems, *J. Math. Anal. Applics* **27**, 417–433 (1969).
35. L. H. BACK, Flow and heat transfer in laminar boundary layers with swirl, *AIAA Jl* 7 (9), 1781–1789 (1969).

APPENDIX

Numerical Calculations

The coupled, integro-differential equations (20) and (21) were rewritten as a system of first order ordinary differential equations (ode's). The following relationship illustrates this transformation. Let $F(I)$ be the Ith first order ode which when integrated once yields the Ith component of the solution vector $Y(I)$. Then the relationships between $F(I)$, $Y(I)$ and the original variables are given by

$F(I)$	Original variable		$Y(I)$
	f	$=$	$Y(1)$
$F(1)$	$=$ f'	$=$	$Y(2)$
$F(2)$	$=$ f''	$=$	$Y(3)$
$F(3)$	$=$ f'''	$=$	$f'''(\eta, Y, F; K, \beta, g_w, S)$
	G	$=$	$Y(4)$
$F(4)$	$=$ G'	$=$	$Y(5)$
$F(5)$	$=$ G''	$=$	$G''(\eta, Y, F; K, \beta, g_w, S)$

where f''' and G'' are obtained from equations (20) and (21) respectively. The integral in equations (20) and (21) was replaced by introducing the following auxilliary ode

$$\int_0^\eta \frac{T}{T_0}\,d\eta = Y(6)$$

$$F(6) = \frac{T}{T_0}.$$

Since the boundary condition equation (14) is nonlinear, another auxiliary ode with linear boundary condition was introduced as follows to be able to use an existing computer code [29] although such a treatment is not necessary in general.

$$f'' \to \left[\frac{-Kf'}{\left(1 + K\int_0^\eta \frac{T}{T_0}\,d\eta\right)}\right] = Y(7)$$

$$F(7) = \frac{K^2 f'\left(\frac{T}{T_0}\right) - Kf''\left(1 + K\int_0^\eta \frac{T}{T_0}\,d\eta\right)}{\left(1 + K\int_0^\eta \frac{T}{T_0}\,d\eta\right)^2}$$

The problem so formulated involves seven ode's and seven boundary conditions at the end points

$$\eta = 0: f = Y(1) = 0, f' = Y(2) = 0, G = Y(4) = 0,$$
$$Y(6) = Y(7) = 0$$
$$\eta = \eta_\infty: G = Y(4) \to 1, f'' = Y(3) \to Y(7)$$

A value of $\eta_\infty = 7$ was chosen to be large enough for the range of parameters considered, e.g. see Fig. 3.

The method used to solve the system of seven ode's is a modified version of the standard "shooting" method. The method, referred to as "multiple or parallel shooting", divides the problem into many problems and then solves all of them simultaneously. The method requires an initial global approximation for each component of the Y vector, as well as guesses for the unknown profile slopes at the wall, $f_w'' = f''(0) = Y(3)$ and $G_w' = G'(0) = Y(5)$. The profiles shown in Fig. 3 for a value of $K = 0$ were chosen in this regard although the method is rather insensitive to the initial global approximation. The method proceeds by integrating the ode vector F from the boundary $\eta = 0$ until the integration of at least one component of the F vector becomes unstable, say at η_1. A variable order, variable step,

Adams type integrator was used [30]. At the location η_1, a breakpoint is inserted. A new problem is then initiated by using the global approximation for $\eta \geqq \eta_1$ similar to the first integration and the ode vector F is integrated again. This process is continued by inserting breakpoints wherever needed until η_∞ is reached. The goal of the "multiple shooting" method is to minimize the vector norm of the residuals at the boundaries $\eta = 0$ and η_∞, and the discontinuities at the breakpoints η_n by adjusting the initial profiles, i.e. the components of the Y vector. A rather powerful version of Newton's method [31] is employed to minimize the residual vector. If the initial global approximation to the Y vector and profile slopes at the wall are poor, the version of Newton's method used will consider a rank deficient change to the solution vector until a change can be made which will minimize the residual vector in a monotonically decreasing manner. The "multiple shooting" method makes no distinction between errors in satisfying boundary conditions and in discontinuities that occur at the inserted breakpoints. Thus, when the largest of these errors is minimized with respect to a tolerance ε (a value of 10^{-5} was used), the method terminates. Further details on this method are given in [32–34] and as applied herein in [29].

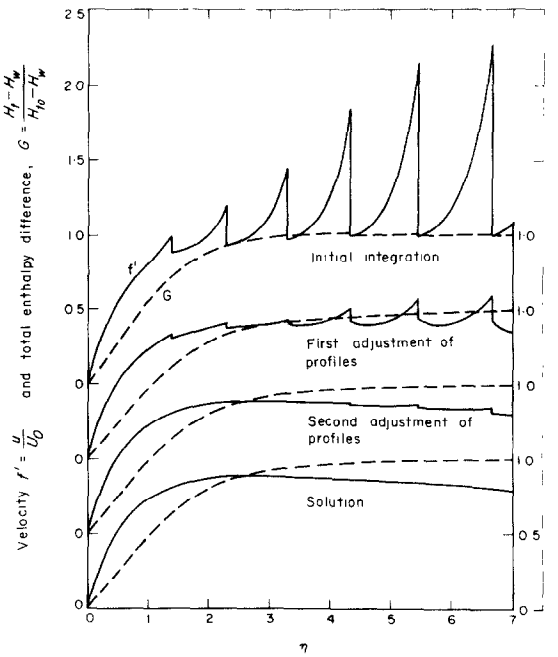

FIG. 7. Progressive development of the solutions: $M_0 = 1$, $\beta = 8{\cdot}54$, $r_c/r_{th} = 0{\cdot}25$, $K = 0{\cdot}12$, $g_w = 0{\cdot}2$, $\gamma = 1{\cdot}2$.

An indication of how the method proceeds is shown in Fig. 7. The difficulty in obtaining solutions as is well known is associated with the momentum equation which dictated the insertion of breakpoints. The number of breakpoints was primarily dependent on the magnitude of the free-stream velocity gradient parameter β, with calculations for larger values of β requiring more breakpoints. In this regard it should be noted that there is a trade-off between the number of breakpoints and the magnitude of the discontinuities at the breakpoints (components of the residual vector). The computation time on a UNIVAC 1108 computer took between one to two minutes for each calculation, i.e. given set of parameters. Solutions could not be obtained with a standard "shooting method", e.g. as used in [9] and [35].

COUCHES LIMITES LAMINAIRES TRANSONIQUES AVEC COURBURE DE LA SURFACE

Résumé—L'effet de courbure de la surface (à la fois longitudinale et transversale) et de gradient transversal de pression associé est étudié analytiquement pour une couche limite laminaire soumise à des gradients de pression dans la direction de l'écoulement. On considère la compressibilité et la variation des propriétés qui résultent du transfert thermique. Des solutions numériques des équations de la couche limite sont obtenues dans le cas d'un écoulement sonique localement similaire au col d'une tuyère pour différentes conditions d'écoulement, diverses formes de tuyères et plusieurs taux de refroidissement pariétal. Quelques solutions ont également été obtenues pour l'écoulement autour du flanc d'un corps à face plate dans un écoulement supersonique. L'effet des divers paramètres qui apparaissent dans les équations traitées par l'application de la transformation de Levy–Mangler est discuté vis-à-vis de l'influence sur les profils de vitesse et d'enthalpie totale et sur les gradients pariétaux de ces profils en relation avec la contrainte tangentielle et le transfert thermique. Une importante découverte est que, pour des nombres de Reynolds au col inférieurs à 10^5, le paramètre de transfert thermique décroît quand le rayon de courbure du col décroît.

LAMINARE ÜBERSCHALL-GRENZSCHICHTEN MIT OBERFLÄCHENKRÜMMUNG

Zusammenfassung—Der Effekt der Oberflächenkrümmung (sowohl longitudinal als auch transversal) und der assoziierte Druckgradient quer durch die Strömung wurden für eine laminare Grenzschicht in

Abhängigkeit vom Druckgradienten längs der Strömung analytisch untersucht. Änderungen der Eigenschaften, die aus der Wärmeübertragung und der Kompressibilität resultieren, wurden in die Betrachtung einbezogen. Numerische Lösungen der Grenzschichtgleichungen wurden für die lokal ähnliche Schallströmung durch die Eintrittsöffnung einer Düse, für eine Reihe von Strömungsbedingungen und für verschieden gestaltete Düsenoberflächen mit unterschiedlichen Werten der Wandkühlung, gewonnen. Einige Lösungen wurden auch für die analoge Strömung um den Bug eines ebenen Körpers in einer Überschallströmung gewonnen. Der Effekt von verschiedenen Parametern in den Gleichungen, herrührend aus der Anwendung, der Levy-Mangler-Transformation, wurde untersucht und diskutiert, wobei ihr Einfluss auf die Geschwindigkeitsprofile, die Profile für die totale Enthalpie und die korrespondierenden Profil-Neigungen der Oberfläche, auf die die Schubspannung und die Wärmeübertragung bezogen sind, beachtet wurden. Wesentlich ist für den Fall, dass die auf die Eintrittsöffnung bezogenen Reynolds-Zahlen kleiner als 10^5 sind, dass der Wärmeübertragungsparameter für den Düsenhals wie der Eintrittsöffnungsradius der Kurvenform abnimmt.

ОКОЛОЗВУКОВЫЕ ЛАМИНАРНЫЕ ПОГРАНИЧНЫЕ СЛОИ ПРИ НАЛИЧИИ КРИВИЗНЫ ПОВЕРХНОСТИ

Аннотация—Аналитически исследуется влияние как продольной, так и поперечной кривизны поверхности и связанного с ней градиента давления поперек потока на ламинарный пограничный слой, который подвергается воздействию продольного градиента давления. Учитывается изменение параметров, вызываемое процессами переноса тепла и сжимаемости. Получены численные решения уравнений пограничного слоя при локально автомодельном звуковом течении через критическое сечение сопла для ряда условий течения и различных форм поверхностей сопла с различной степенью охлаждения стенки. Получено также несколько решений для аналогичного сверхзвукового обтекания кромки поперечно обтекаемого тела. Исследуется влияние различных параметров, появляющихся в уравнениях в результате применения преобразования Леви-Манглера, и рассматривается их влияние на профили скорости и полной энтальпии, а также на напряжение трения и поток тепла через стенку. Сделан важный вывод о томб что при значениях числа Рейнольдса меньше 10^5 параметр теплообмена в критическом сечении сопла уменьшается по мере уменьшения радиуса его кривизны.